SAND2017-8614R

Sandia National Laboratories

Operated for the United States Department of Energy
by National Technology and Engineering Solutions
of Sandia, LLC.

Albuquerque, New Mexico 87185-0101
Livermore, California 94551-0969

*date:* August 10, 2017

*to:* Allen Roach

*from:* Grace X. Gu (1554), Judith A. Brown (1554), Joseph Bishop (1554)

*subject:* Adjoint-based optimization of mechanical performance in polycrystalline materials and structures through texture control

## ABSTRACT

The texture of a polycrystalline material refers to the preferred orientation of the grains within the material. In metallic materials, texture can significantly affect the mechanical properties such as elastic moduli, yield stress, strain hardening, and fracture toughness. Recent advances in additive manufacturing of metallic materials offer the possibility in the not too distant future of controlling the spatial variation of texture. In this work, we investigate the advantages, in terms of mechanical performance, of allowing the texture to vary spatially. We use an adjoint-based gradient optimization algorithm within a finite element solver (COMSOL) to optimize several engineering quantities of interest in a simple structure (hole in a plate) and loading (uniaxial tension) condition. As a first step to general texture optimization, we consider the idealized case of a pure fiber texture in which the homogenized properties are transversely isotropic. In this special case, the only spatially varying design variables are the three Euler angles that prescribe the orientation of the homogenized material at each point within the structure. This work paves a new way to design metallic materials for tunable mechanical properties at the microstructure level.

*Sandia National Laboratories is a multimission laboratory managed and operated by National Technology and Engineering Solutions of Sandia, LLC., a wholly owned subsidiary of Honeywell International, Inc., for the U.S. Department of Energy's National Nuclear Security Administration under contract DE-NA0003525.

## INTRODUCTION

Additive manufacturing of metallic materials, which involves layer-wise consolidation of feedstock materials in the form of powder, wire, or sheet using various energy sources to form complex parts, is undergoing significant advances. As new feedstock materials keeps growing, academic, government, and industrial research institutions become increasingly interested in the field of metallic additive manufactured materials and its applications. Compared to traditional manufacturing methods, additive manufacturing introduces new potential for local microstructure control by tuning process parameters in different parts of the build. With microstructure considerably affecting properties, such as elastic moduli, plastic deformation, strain hardening, and fracture toughness, control of microstructure allows control of material properties [1, 2].

Previous works have already shown that some microstructure or texture control of metallic additive manufactured materials can be realized using methods such as electron beam method (EBM) and directed energy deposition (DED) methods. Raghavan et al. recently used an innovative process control method that allows the operator to change melting conditions in which a build with columnar or equiaxed microstructure was achieved on-demand [3]. Makiewicz et al. used model-based process parameters with a DED technique to achieve a homogeneous microstructure that led to improved fatigue properties [4]. Dinda et al. reports a study using a laser-aided direct metal deposition process that can produce texture controlled structures on a polycrystalline substrate by adjusting the laser beam scanning velocity [5]. Dehoff et al. presented the growth of highly mis-oriented equiaxed grains outlining the letters D, O, and E through the thickness of a block comprised of columnar oriented grains made of a nickel base superalloy. These works on the process side in metallic additive manufacturing opens the possibility of optimizing the microstructure to tailor of mechanical properties for a desired application. To take advantage of this developing capability, spatially variable material properties must be considered a design variable in optimization of additive parts.

Optimization of materials for properties such as compliance, stiffness, thermal expansion coefficient, and fracture toughness is widespread in literature. Various optimization methods can be divided into two categories: gradient based and heuristic based (genetic, greedy, simulated annealing). Most topology optimization works using gradient based methods focused on the larger scale material properties, rather than starting at the microstructure properties [7, 8]. For instance, Gaynor et al. used multiple material topology optimization to create compliant structures [9]. Buhl et al. used a gradient based approach of Method of Moving Asymptotes (MMA) to optimize for stiffness in the structure [10]. Larsen et al. used a numerical topology optimization method to design material structures with negative Poisson's ratio (NPR) [11]. Most optimization work for fiber reinforced composites lies in optimizing the angle in which the plies are stacked using genetic algorithms [12, 13, 14]. However, optimization efforts that include spatially variable material properties, which are governed by local microstructure, as a design variable are so far very limited.

Here, we use an adjoint-based gradient optimization algorithm paired with finite element solvers to find optimal material orientations and positions to minimize quantities of interest of a metallic additive manufactured structure. This work paves a new way to design metallic materials for tunable mechanical properties at the microstructure level. This memo is organized as follows. The finite element modeling (including model set up, boundary conditions, and material properties) and adjoint-based optimization method is described in Section 2. Results of simulation and optimization is discussed in Section 3. Optimal material orientations spatially in a 2D system is explored and analyzed for various objective functions. Additionally, preliminary results of the 2D system expanded to 3D is also investigated. Conclusions and future work is given in Section 4.

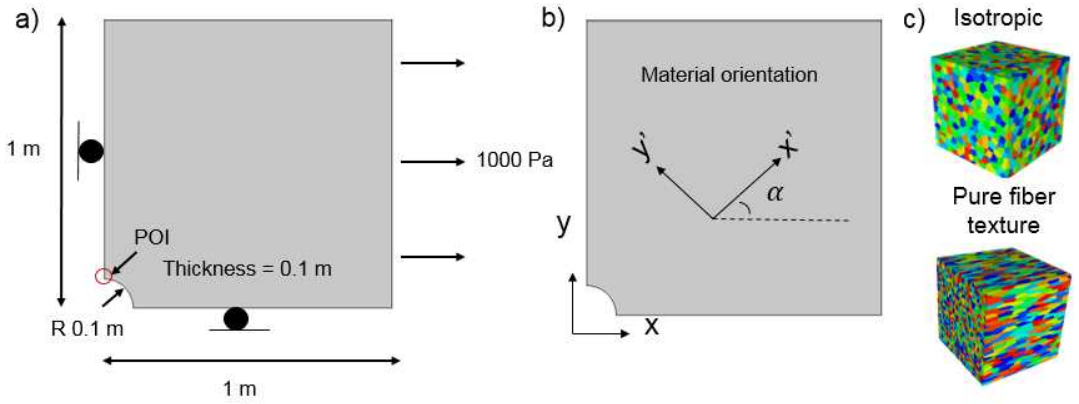


**Figure 1: Inputs into model.** a) Quarter geometry used due to symmetry with dimensions labelled. The loading for the problem at hand is in tension with a boundary load of 1000 Pa. POI is point of interest and is considered the point of maximum stress. b) Local rotated orientation is specified in model to define the material orientation. c) Representative volume elements of the polycrystalline microstructure used to obtain homogenized elastic properties: isotropic (no texture, top) and transversely isotropic (pure fiber texture, bottom).

## 1. METHODS

To obtain spatially optimal material orientations in an AM structure, a finite element solver combined with optimization software is used. Comsol Multiphysics [15] is used for both optimization and structural finite element analysis. This software is used because of its capability to incorporate adjoints in its optimization methods to efficiently solve problems. This work considers a hole in a plate structure. The hole essentially functions as an undesirable byproduct (stress concentrator) and one goal of the optimization is to mitigate the maximum stress point along the hole. Another goal is to minimize the compliance of the structure. The methods used here could potentially be extended to look at cracks (edge, center) in structures which also have stress concentrations at the crack tips.

### 1.1 Finite element Analysis

#### 1.1.1 Model set-up and boundary conditions

The model problem studied in this work is a simple two-dimensional hole in a plate geometry with dimensions outlined in Fig. 1. The plate is considered thin compared to the rest of the other dimensions so plane stress conditions are used. A quarter model is used due to symmetry where symmetry boundary conditions are imposed on the two boundaries. The mesh shown in Appendix Fig. A1 is chosen based on computational efficiency and a mesh convergence study shown in Appendix Fig. A1. A normal traction of 1000 Pa is applied in the *x*-direction. Additionally, this work assumes displacements are in the linear elastic regime of the material.

| | Elastic modulus [GPa] | | | Poisson's ratio [-] | | | Shear modulus [GPa] | | |
|---|---|---|---|---|---|---|---|---|---|
| | $E_{11}$ | $E_{22}$ | $E_{33}$ | $\nu_{12}$ | $\nu_{23}$ | $\nu_{13}$ | $G_{12}$ | $G_{23}$ | $G_{13}$ |
| Isotropic | 198 | 198 | 198 | 0.29 | 0.29 | 0.29 | 76.5 | 76.5 | 76.5 |
| Pure Fiber Texture | 143 | 143 | 90.9 | 0.11 | 0.62 | 0.62 | 58 | 126 | 126 |

**Table 1: Homogenized effective material properties** used in model includes elastic moduli, Poisson's ratios, and shear moduli.

### 1.1.2 Material properties

The material considered here is an additively manufactured 304L stainless steel. Material properties are obtained by performing computational homogenization of representative volume elements (RVE) based on microstructure features observed in AM metals and welds [16]. The RVE's are shown in Fig. 1. A microstructure obtained from an electron backscatter diffraction (EBSD) image of a 304L stainless steel laser weld works as a basis for the RVE grain morphology (add reference). The RVE used has a <100> fiber texture that has been observed experimentally in weld and AM microstructures [16]. This produces homogenized properties that are transversely isotropic. For comparison, we also consider a set of homogenized isotropic material properties obtained from a RVE containing equiaxed grains with uniformly random orientations (no preferred orientation and no texture) [16]. Both sets of material parameters are shown in Table 1.

The material coordinate system is shown in Fig. 1, where $\alpha$ is the angle between the material coordinate system x', y' and the global coordinate system X,Y. For this study, we study three optimization cases:

1. $\alpha$ is varied in a spatially homogeneous material
2. $\alpha$ is varied in a spatially heterogeneous material
3. $\alpha$ and $p$ is varied in a spatially heterogeneous material

where $p$ is an additional parameter that varies the degree of transverse isotropy in the material stiffness tensor. For this case #3, the elasticity tensor $C$ is composed of the transversely isotropic portion ($C_{TI}$) and also the isotropic portion ($C_I$) as

$$C = p * C_{TI} + (1 - p) * C_I \quad (1)$$

where $p$ varies between 0 and 1 and $C_{TI}$ and $C_I$ are the elastic constants given in Table 1 and the elasticity matrices are shown in the Appendix. Note that this is a very simplified way to vary the elastic properties. A more rigorous approach would be to allow the texture to vary from "none" to "pure fiber" and then rerun an RVE simulation to recover the homogenized elastic constants. This would involve doing this for several "$p$" values and then fitting an interpolation curve to each elastic constant so that it could be used by COMSOL.

**2.2 Optimization**

2.2.1 Objective functions

Two main objective functions that are explored in this study are shown in Eq. 2. The first is strain energy ($Q_1$), which is defined as the integral of strain energy density ($W_S$) over the entire domain. Strain energy balances the work done by the applied load. As a result, minimizing strain energy minimizes the displacement induced at the points where load is applied, effectively minimizing the compliance of the structure, and maximizing its stiffness. The second is the von Mises stress ($Q_2$) at the point of interest (POI) labeled in Fig. 1, which is the maximum stress point on the hole for a general isotropic material. The idea behind the second objective function is to dissipate and decrease the stress at a critical point in the system, which is the maximum stress point. The variable we are optimizing in the problem is $\alpha(x, y)$, the local orientation of the material coordinate system, mentioned in Section 2.1.2.

$$\begin{aligned} Q_1 &= \int_\Omega W_S d\Omega \\ Q_2 &= \sigma_{VM}(\text{at POI}) \end{aligned} \quad (2)$$

2.2.2 Adjoint-based gradient method

To optimize our system, we use a gradient-based method from the Comsol optimization toolbox called Method of Moving Asymptotes (MMA). This is an iterative method that generates and solves a convex subproblem within each iteration [17]. This method uses upper and lower moving asymptotes to adjust the curvature of the approximate functions, with the selection of the moving asymptotes as largely heuristic. Additionally, adjoint methods are necessary to solve for values of $\alpha(x, y)$ that are allowed to vary spatially within the structure [15, 18]. The adjoint method is a numerical method for efficiently computing the gradient of a function or operator in a numerical optimization problem. It formulates the

gradient of a function towards its parameters in a constraint optimization form. The optimization problem requires:

$$\frac{dQ}{d\alpha} = 0 \tag{3}$$

where $Q$ is the objective function (two of which are mentioned in Eq. 2) and $\alpha$ is the angle variable in the optimization problem as shown in Fig. 1. Therefore the equation that is needed to be solved is

$$\frac{dQ}{d\alpha} = \frac{dQ}{du}\frac{du}{d\alpha} \tag{4}$$

where $u$ is the position of all the angles. Now, we introduce an adjoint variable defined as

$$\lambda^T = \frac{dQ}{du}K^{-1}(\alpha) \rightarrow \frac{dQ}{du} = \lambda^T K(\alpha) \tag{5}$$

where $\lambda$ is the adjoint variable and $K$ is the stiffness matrix. Now that we have the equation for $\frac{dQ}{du}$, we now need to solve for $\frac{du}{d\alpha}$. We know that

$$K(\alpha)u = F \tag{6}$$

where F are the forces applied to the system. Differentiating Eq. 6, we get

$$K(\alpha)\frac{du}{d\alpha} + \frac{dK(\alpha)}{d\alpha}u = \frac{dF}{du} = 0 \tag{7}$$

This means that

$$\frac{du}{d\alpha} = -K(\alpha)^{-1}\frac{dK(\alpha)}{d\alpha}u \tag{8}$$

Now, the components from Eq. 5 and Eq. 8 can be combined into Equation 4 to result in

$$\frac{dQ}{d\alpha} = \frac{dQ}{du}\frac{du}{d\alpha} = (\lambda^T K(\alpha)) * (-K^{-1}\frac{dK(\alpha)}{d\alpha}u) = -\lambda^T\frac{dK(\alpha)}{d\alpha}u \tag{9}$$

This is the method of adjoints used in the Comsol manual [15] which we use to solve for spatially varying material orientations. The adjoint method aided in eliminating the inverse stiffness matrix ($K$), which is very expensive to solve for computationally.

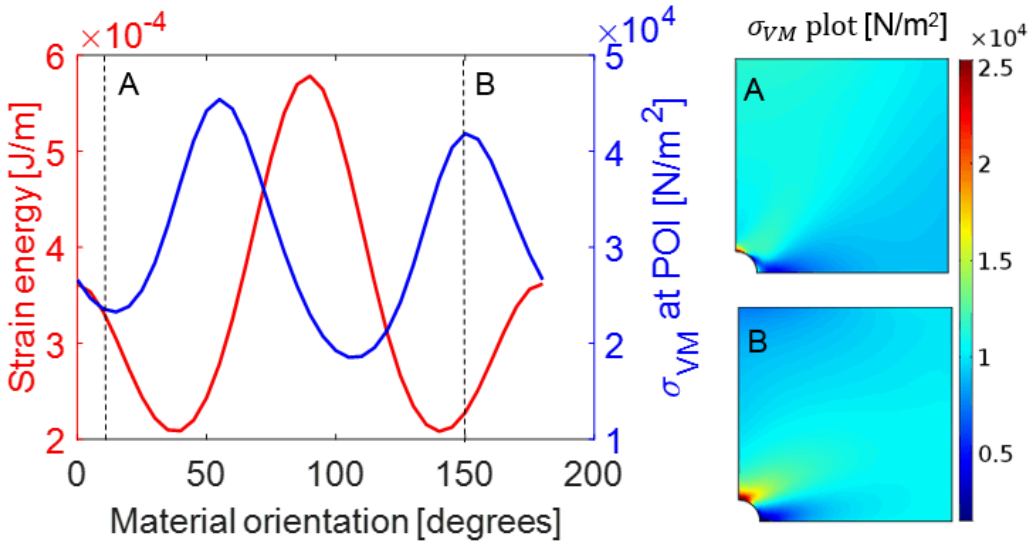


**Figure 2: Parametric sweep of material orientations.** Strain energy and von Mises stress varies with material orientations. Von Mises stress plots for material orientations at locations A (15 degrees) and B (150 degrees) shown on the right depicts differences in stress contours with orientation.

## 3. RESULTS

### 3.1 Parametric sweep

To demonstrate the effects of material orientation on mechanical properties, a parametric sweep study of various material angles ($\alpha$) is performed. The same angle is assumed for all positions in the structure and a forward analysis of various material orientations is executed. Results are shown in Fig. 2. It can be seen that both the properties of strain energy (Q1 from Eq. 2) and von Mises stress (Q2 from Eq. 2) vary with material orientation. The curve for strain energy is very symmetric while the curve for von Mises stress at the selected point of interest is not. The reason for this is that the equation for solving strain energy is an integral over the entire material domain while the von Mises stress objective is taken from just a point. This knowledge of symmetry is critical for the optimization step in which for strain energy the angles should be constrained from 0 to 90 degrees while for von Mises, the angles should be constrained from 0 to 180 degrees. Additionally, it can be seen that for both properties, $\alpha = 0$ and $\alpha = 180$ output the same answer, which is true because they are essentially in the same plane. Two points on the von Mises curve are compared, A and B, with A at $\alpha = 15$ degrees and B at $\alpha = 150$ degrees. Comparing the von Mises plots for both points shown in Fig. 2, it can be seen that the stress plots are very different for the two angles. At point B, there is higher stress and a larger stress concentration around the hole compared to point A. This parametric sweep of the forward analysis shows that material orientation has a significant effect on the objective functions.

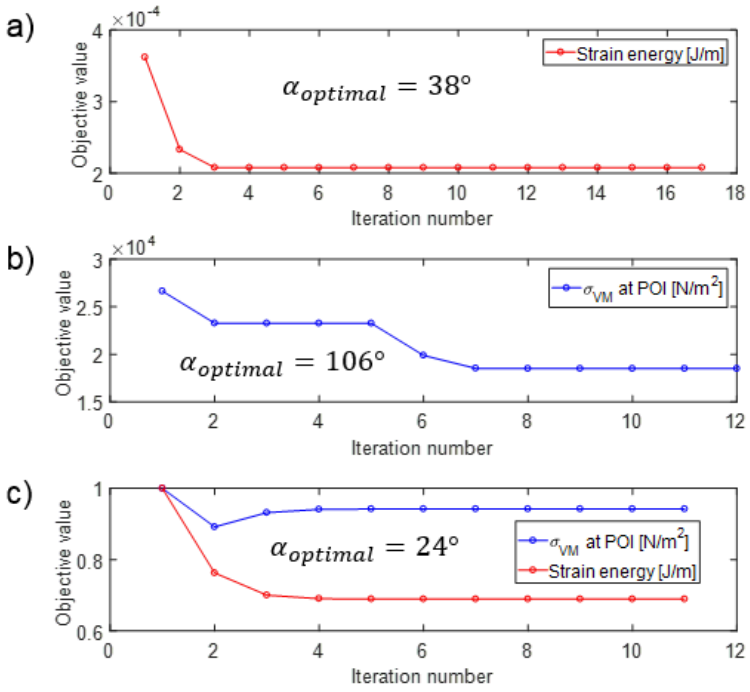


**Figure 3: Optimization with spatially homogeneous properties.** Objective value as a function of iteration number in the simulation is shown for a) strain energy, b) von Mises stress at POI, and c) both strain energy and von Mises stress at POI (multi-objective optimization using equal weighting). Optimal angles for all three scenarios are shown in the plot.

### 3.2 Optimization with spatially homogeneous properties

Next we perform an optimization study to determine the optimal material orientation for the structure with spatially homogeneous properties and constant material stiffness. For the first objective function of strain energy, $\alpha$ is constrained from 0 to 90 degrees due the symmetry in the parametric sweep. From the parametric sweep, it can be seen that the minimal point is around $\alpha$ = 40 degrees (Fig. 2). After optimization, starting with an initial point of $\alpha$ = 0, we discover that the optimal angle is $\alpha$ = 38 degrees. This helps to verify that the optimization method is working correctly and within the results of our forward analysis. Fig. 3 shows the objective value of strain energy decreasing with each iteration and eventually converging into a solution. For the second objective of von Mises stress, we constrain $\alpha$ from 0 to 180 degrees. From the parametric sweep, it can be seen that the minimal point is around 110 degrees. Fig. 3 shows the objective value decreasing with each iteration and eventually converging into a solution of $\alpha$ = 106 degrees.

In addition to studying these two objectives optimized separately, we study multi-objective optimization for applications that need to have optimal values for both objectives. In order to do multi-objective optimization, we use a sum of the objectives using equal weighting, denoted as $Q = Q_1 + Q_2$. The properties are first normalized to prevent any bias from the magnitude of the properties with different units using solutions from $\alpha$ = 0. Fig. 3 shows the objective value versus iteration and converging for both properties. It can be seen that in the beginning, both properties were able to decrease, however, at

some point the objective function for von Mises stress had to increase to allow for even more decrease in strain energy, which consistently decreases with iteration. This shows that tradeoffs are needed to find an optimal value most beneficial to the system. The optimal angle for the multi-objective problem is $\alpha$ = 24 degrees. It is important to note that for different applications, this equal weighting can be adjusted to fit a certain application that may require better performance in one of the objectives.

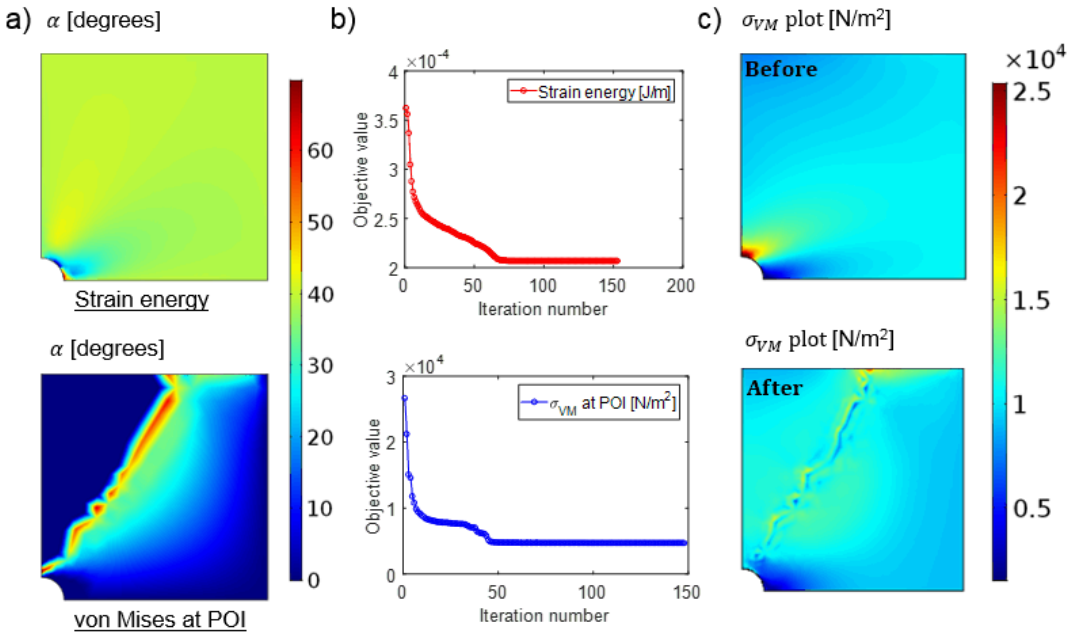


**Figure 4: Optimization with spatially heterogeneous properties.** a) Optimal angle color plot spatially is shown for strain energy and von Mises at POI. b) Objective value as a function of iteration number is minimized and converged for strain energy and von Mises at POI. c) Before optimization and after optimization von Mises plots optimized to minimize von Mises at POI shows much lower stress for the after optimization stage.

### 3.3 Optimization with spatially heterogeneous properties

The previous section discussed an optimal material angle that is uniform in the entire structure. However, allowing the material orientation angle to vary spatially will better suit the evolving capability of additive manufacturing to produce point-wise material control within a printed structure. Using the method of adjoints allows us to efficiently solve for optimal angles at each point in the geometry (Section 2). For the strain energy objective function, Fig. 4 shows a colorplot of the optimal angles in degrees. It can be seen that most parts of the geometry far away from the hole area is in the regime of $\alpha$ = 40 degrees, which is very close to the optimal angle obtained from the optimization of spatially homogeneous properties of $\alpha$ = 38 degrees. Near the hole, the angles seem to vary much more to decrease the strain energy of the system and mitigate the effects of the hole. Also shown in Fig. 4 is the strain energy objective value decreasing with iteration and eventually converging to a value.

For the von Mises objective function, Fig. 4 shows a colorplot of the optimal angles and it can be seen that near the POI, the angles start to deviate following the region of maximum shear stress that follows a

45 degree angle from the hole, trying to lower the stress at the point. Additionally, the von Mises stress plot before optimization is shown for $\alpha$ = 150 degrees compared to the von Mises stress plot with optimal angles after optimization. It can be viewed that with optimization, all the stress that was near the hole is dissipated and the stress is much more distributed in the material, lessening the effects of the hole.

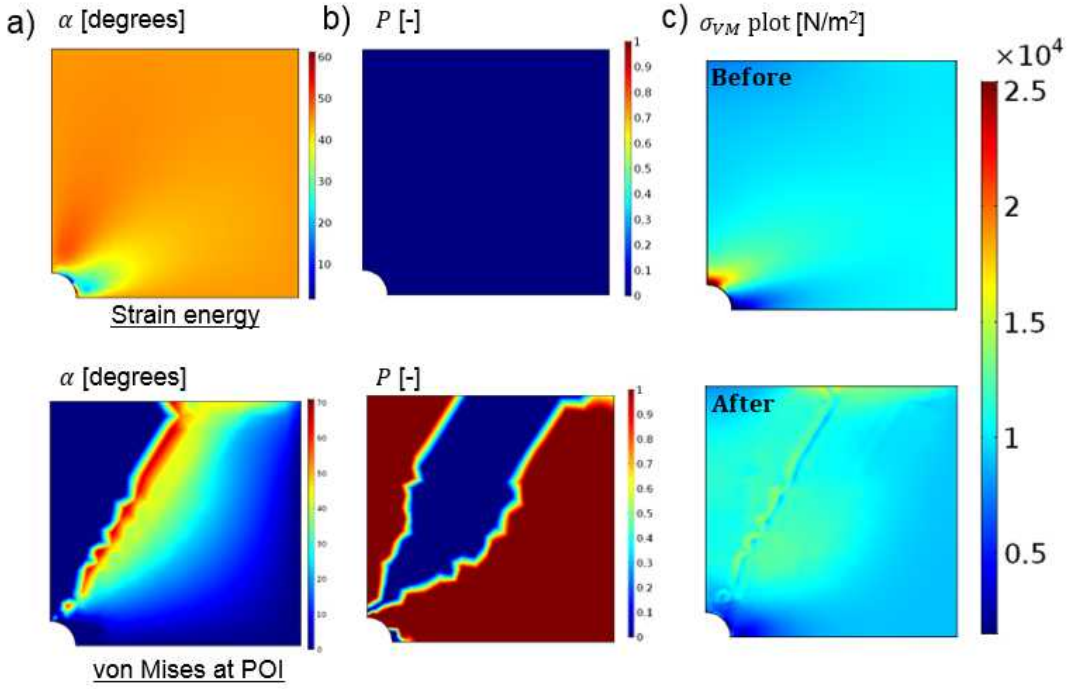


**Figure 5: Optimization of variable elastic properties.** Optimal angle and variable *P* (degree of isotropy discussed in Methods section) spatially in material, and resulting von Mises stress plot is shown for the objective function of a) strain energy and b) von Mises stress at POI.

### 3.4 Optimization with variable elastic properties

The three previous studies have assumed constant stiffness properties; however, the AM process potentially offers the capability to vary both stiffness properties and material orientation throughout a printed structure. Thus, another variable is added to consider material variation in the system. We introduce another variable $p$ to take into account the degree of isotropy present in the stiffness matrix (Eq. 1). So if $p = 0$, the material is isotropic, and if $p = 1$, then the material is the transversely isotropic solution representative of a pure fiber texture. $p$ in between those two regimes allows for intermediate materials in between those two extremes. Now for this problem, there are two variables, $\alpha$ and $p$.

For the objective of strain energy, optimal angles and $p$ spatially is shown in Fig. 5; it can be seen that the angles plot look similar to the previous spatially heterogeneous properties plot. For $p$ spatially, the optimal value is $p = 0$ everywhere in the geometry, meaning it obtains the isotropic solution. Since strain energy is correlated to stiffness and since the isotropic solution has high values for elastic modulus in most of the directions, this solution makes sense. For the von Mises objective, it can be seen that the

solution for angles look quite similar as before in section 3.3. As for $p$, the variation in $p$ also lies around the 45 degree angle between the hole and the edge of the plate. The von Mises stress plot shows more dissipated stress from the hole where maximum stress originally was located.

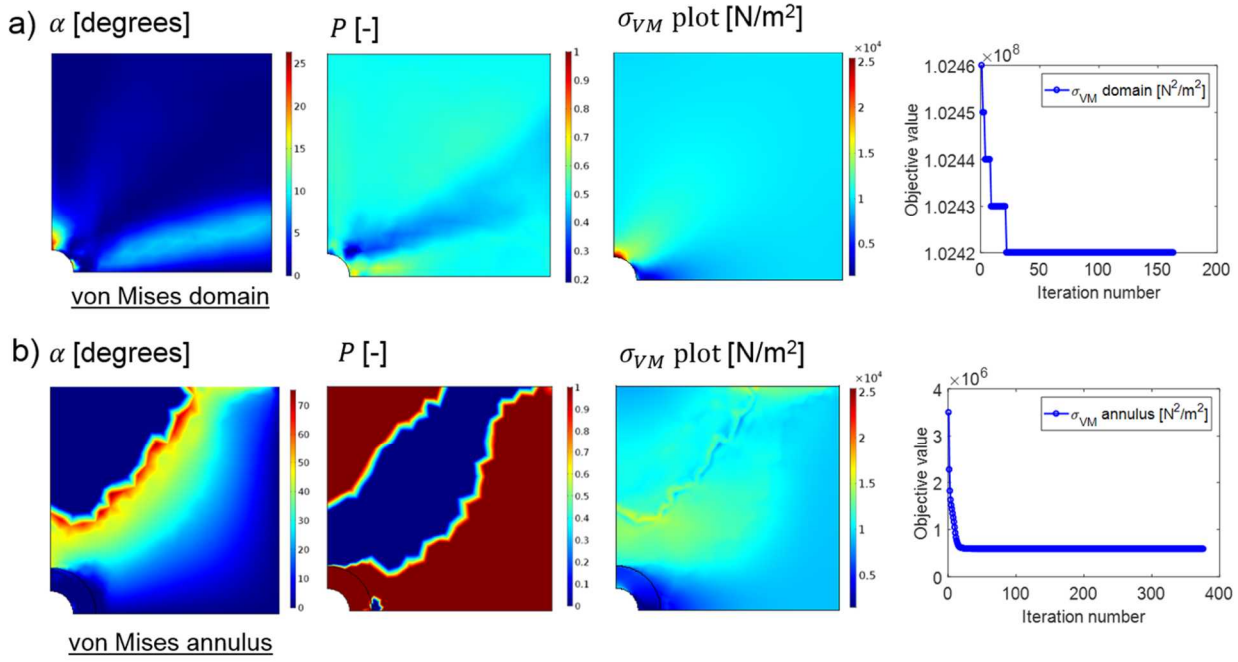


**Figure 6: Varying objective functions for von Mises stress.** Optimal angle and variable $p$ (degree of isotropy discussed in Methods section) spatially in material, resulting von Mises stress plot, and objective value with iteration number is shown for the objective function of integrating the square of von Mises stress a) over the entire domain and b) over an annulus around the hole.

### 3.5 Variation of von Mises objective functions

In the previous section, the von Mises objective function was solved at a point. This method works in applications where it is necessary to dissipate the stress at a point. However, in some applications, average stress over a domain is more important. Here, we study two additional cases, an averaged von Mises stress over the entire domain and an averaged von Mises stress over an annulus with radius 0.1 m around the hole (shown in Appendix Fig. A2). For the entire domain objective function, we integrate the square of von Mises over the entire geometry. The results are shown in Fig. 6. For this objective function, the band of angles along the 45 degree line between the hole and plate edge is no longer there, and the same applies for the variable $P$. Looking at the von Mises stress plot, there still exists very high stress around the hole, meaning that the stress is not dissipated. Additionally, it can be seen that with iteration, the objective value does not decrease much for this objective value. From this analysis, it looks like the angle effects just cancel each other out when integrating over the entire domain rather than a region of interest. For the average von Mises stress around an annulus, we integrate the square of von Mises stress over a region one radius value larger than the radius of the hole. Results for this objective function is shown in Fig. 6. It can be seen that the angle profile is shifted from before when von Mises stress was defined at a point. This average method helps to shift the stress away from the region of

interest instead of just the point of interest. It can also be seen that with iteration, the objective value is decreasing and from the von Mises stress profile the high stress values near the region of interest disappears. Differences occur when looking at the entire domain.

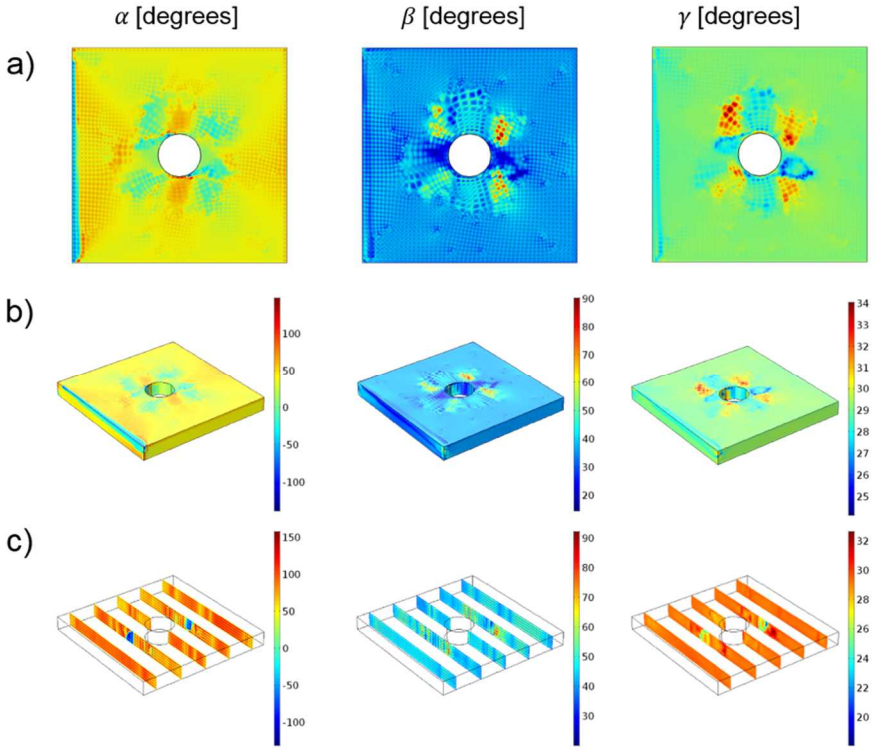


**Figure 7: Optimal Euler angle orientations for strain energy.** a) Top view b) 3D view and c) Sliced view for cross-sectional angles.

### 3.6 Preliminary three-dimensional model results

We extend our method of adjoints and gradient optimization to study a three-dimensional (3D) system with a hole, with dimensions shown in Appendix Fig. A3. The height is 2 meters long, width is 2 meters wide, and thickness is 0.2 meters. A 3D model allows the study of the three Euler angles in a material system, with Euler angle notation from Comsol manual [15] shown in Appendix Fig. A4. This optimization problem has three design variables, which are denoted as $\alpha(x, y, z)$, $\beta(x, y, z)$, and $\gamma(x, y, z)$. The same optimization approach and objective functions as the 2D system is used for the 3D system. The main difference is that the 2D system has one design variable, while the 3D system has three. A forward analysis of the 3D system is shown in Appendix Fig. A4. It can be seen that in the location near the hole there is high stress concentration similar to the 2D case but through the thickness direction. Running the optimization scheme with this problem, there will be three colorplots to look at with optimal $\alpha$, $\beta$, and $\gamma$ angles shown in Fig. 7 for strain energy objective function. Different views of the colorplot is shown in Fig. 7, one of which is the capability of Comsol to view the optimal angles along a cross-section in different slices of the material. Appendix Fig. A5 shows the strain energy as a function of optimization iteration number. Fig. 8 compares the displacement along the top of the

material between the forward analysis without optimization and after optimization. It can be seen that the maximum displacement has reduced by approximately half using the optimized Euler angles shown in Fig. 7. Total displacement is used here to visualize strain energy reduction because as mentioned in the Methods section, strain energy is correlated to compliance and this problem seeks to minimize compliance of the system.

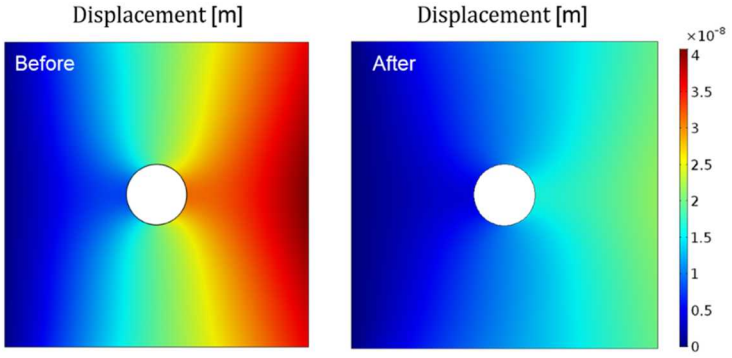


**Figure 8: Before and after** displacement field for minimizing strain energy

Von Mises stress objective function is solved for using an annulus around the hole. The von Mises stress at a point objective function cannot apply here as the model now includes a thickness. From the 2D model, we realize that integrating the von Mises stress over the entire domain does not improve the objective function very much. As a result, for the 3D case, we integrate an annulus domain around the hole to solve for the von Mises objective function. Optimized Euler angle solutions are shown in Fig. 9. The lines in the optimization stress field shows the annulus domain where integration took place. Appendix Fig. A4 shows the von Mises stress as a function of optimization iteration number. We compare the before optimization von Mises stress plot around the hole area to after optimization and can see that most of the stress through the thickness is mitigated. Extending our problem to 3D shows that after optimization, the material thickness area has a heterogeneous angle profile.

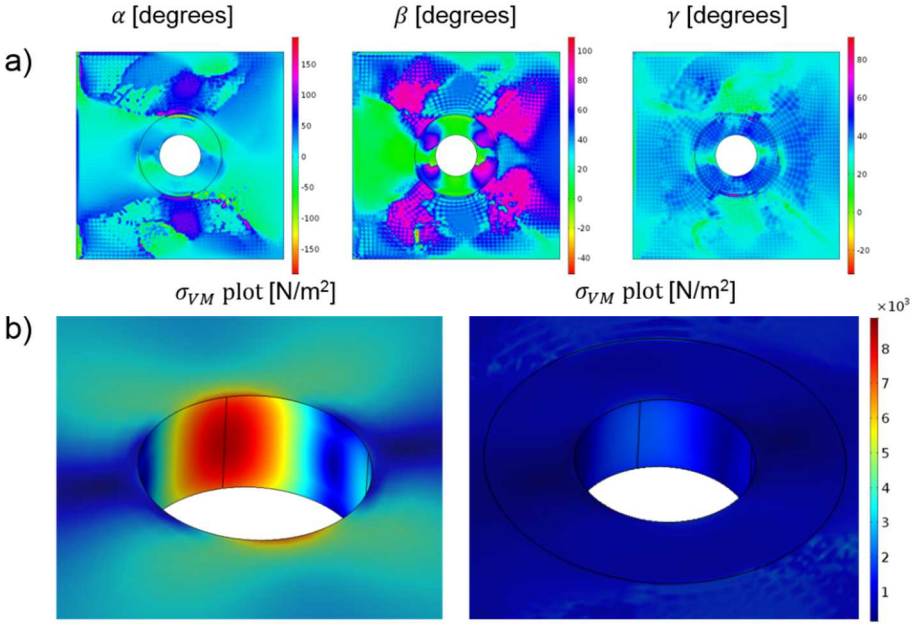

**Figure 9: Euler angle solutions** for minimizing von Mises stress. a) Euler angle solutions b) Before (Left) optimization von Mises stress plot around the hole thickness is compared to after (Right) optimization solution.

## 4. CONCLUSIONS AND FUTURE WORK

In this work, we present a technique to optimize material orientations of polycrystalline materials using a combination of finite element analysis and gradient-based optimization. To efficiently solve for the optimal material orientations, an adjoint based design optimization method is used. Optimal material angles for a spatially homogeneous and spatially heterogeneous material are optimized for quantities of interest, such as compliance and von Mises stress. Additionally, we look into a combination of stiffness tensor and material orientation variables effect on optimized structures, as the AM processes potentially offers the capability to vary both. The methods and framework proposed here can be extended to study other structures and designs and offers a tool to create optimized geometries with varying material orientations. It is worth mentioning that for this study, we considered a linear elastic model and optimized behavior in the small-strain regime. An expansion of this work could be to extend the approach to explore nonlinear behavior, such as plasticity. Another extension can be to combine material orientation with topology optimization.

## References

[1] Das, Suman, David L. Bourell, and S. S. Babu. "Metallic materials for 3D printing." MRS Bulletin 41.10 (2016): 729-741.

[2] Ding, Y., et al. "Microstructure and mechanical property considerations in additive manufacturing of aluminum alloys." *MRS Bulletin* 41.10 (2016): 745-751.

[3] Raghavan, Narendran, et al. "Numerical modeling of heat-transfer and the influence of process parameters on tailoring the grain morphology of IN718 in electron beam additive manufacturing." *Acta Materialia* 112 (2016): 303-314.

[4] Makiewicz, K., et al. "Microstructure Evolution During Laser Additive Manufacturing of Ti6A14V Alloys." *Proc. Int. Conf. Trends Weld. Res. Chicago, IL*. 2012.

[5] Dinda, G. P., A. K. Dasgupta, and J. Mazumder. "Texture control during laser deposition of nickel-based superalloy." *Scripta Materialia* 67.5 (2012): 503-506.

[6] Dehoff, R. R., et al. "Site specific control of crystallographic grain orientation through electron beam additive manufacturing." *Materials Science and Technology* 31.8 (2015): 931-938.

[7] Zegard, Tomás, and Glaucio H. Paulino. "Bridging topology optimization and additive manufacturing." *Structural and Multidisciplinary Optimization* 53.1 (2016): 175-192.

[8] Eschenauer, Hans A., and Niels Olhoff. "Topology optimization of continuum structures: a review." *Applied Mechanics Reviews* 54.4 (2001): 331-390.

[9] Gaynor, Andrew T., et al. "Multiple-material topology optimization of compliant mechanisms created via PolyJet three-dimensional printing." *Journal of Manufacturing Science and Engineering* 136.6 (2014): 061015.

[10] Buhl, Thomas, Claus BW Pedersen, and Ole Sigmund. "Stiffness design of geometrically nonlinear structures using topology optimization." *Structural and Multidisciplinary Optimization* 19.2 (2000): 93-104.

[11] Larsen, Ulrik Darling, O. Signund, and S. Bouwsta. "Design and fabrication of compliant micromechanisms and structures with negative Poisson's ratio." *Journal of microelectromechanical systems* 6.2 (1997): 99-106.

[12] Soremekun, G., et al. "Composite laminate design optimization by genetic algorithm with generalized elitist selection." *Computers & structures* 79.2 (2001): 131-143.

[13] Le Riche, Rodolphe, and Raphael T. Haftka. "Optimization of laminate stacking sequence for buckling load maximization by genetic algorithm." *AIAA journal* 31.5 (1993): 951-956.

[14] Lin, Ching-Chieh, and Ya-Jung Lee. "Stacking sequence optimization of laminated composite structures using genetic algorithm with local improvement." *Composite structures* 63.3 (2004): 339-345.

[15] Multiphysics, C. O. M. S. O. L. "Modeling Software." *User Manual* (2016).

[16] Brown, Judith A., and Joseph E. Bishop. "Quantifying the impact of material-model error on macroscale quantities-of-interest using multiscale a posteriori error-estimation techniques." *MRS Advances* 1.40 (2016): 2789-2794.

[17] Svanberg, Krister. "The method of moving asymptotes—a new method for structural optimization." *International journal for numerical methods in engineering* 24.2 (1987): 359-373.

[18] Choi, Kyung K., and Nam-Ho Kim. *Structural sensitivity analysis and optimization 1: linear systems*. Springer Science & Business Media, 2006.

## Appendix

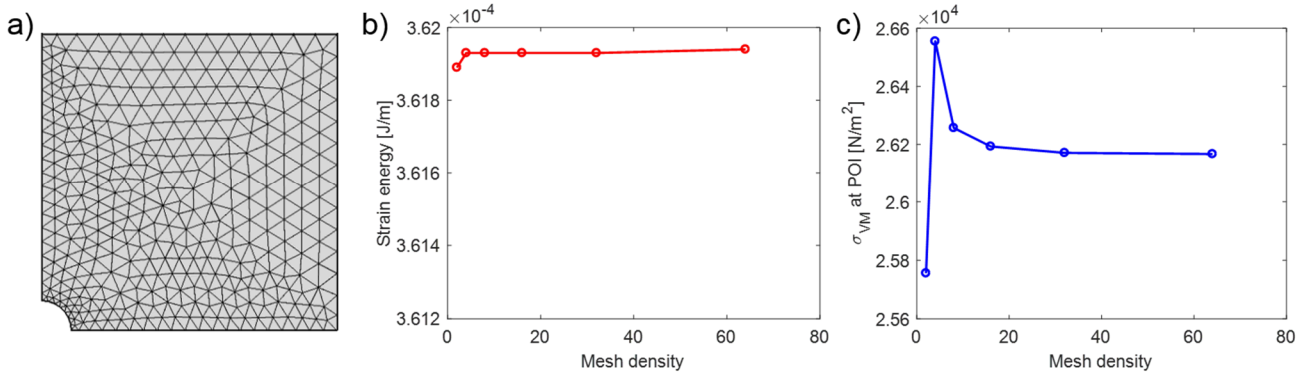


**Fig. A1: Meshing details**. a) Mesh used in study b) Mesh convergence study for the two objective functions.

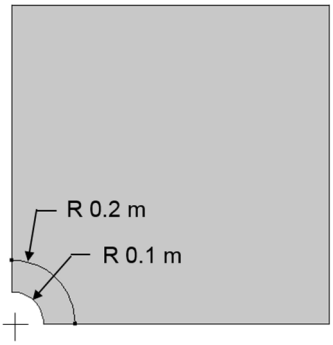


**Fig. A2: Annulus domain** used for averaged von Mises stress calculation

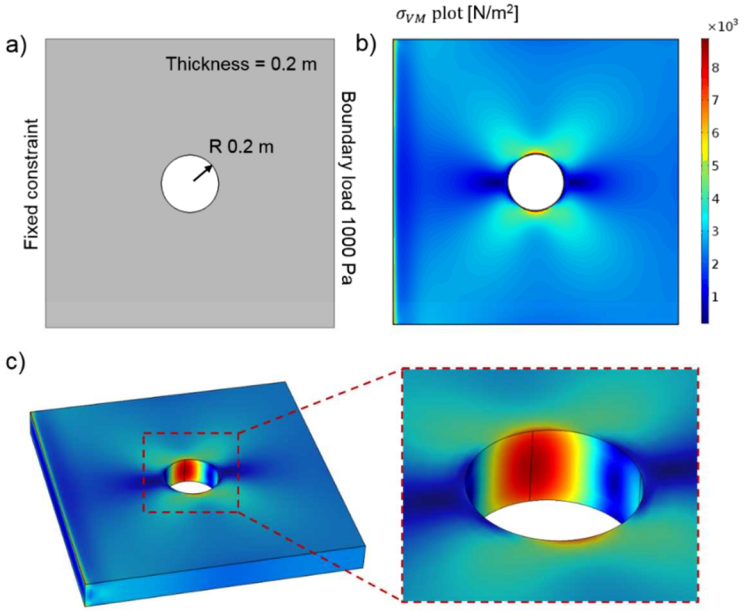


**Fig. A3: Forward analysis for 3D model**. a) Dimensions of model b) Von Mises stress profile from top view c) Von Mises stress profile zoomed in the hole thickness area

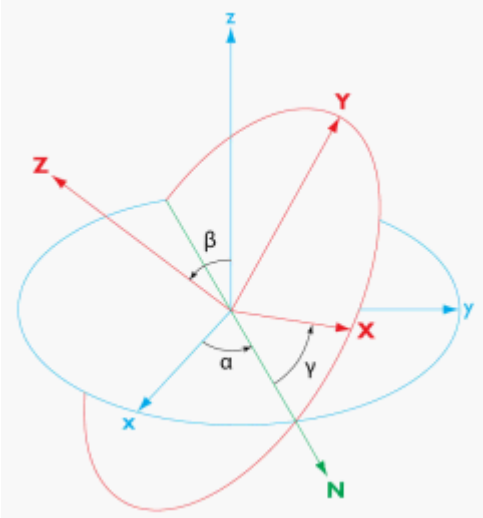


**Figure A4: Schematic** of Euler angles α, β, and γ where lowercase xyz represents the original coordinate system and uppercase XYZ represents the rotated coordinate system.

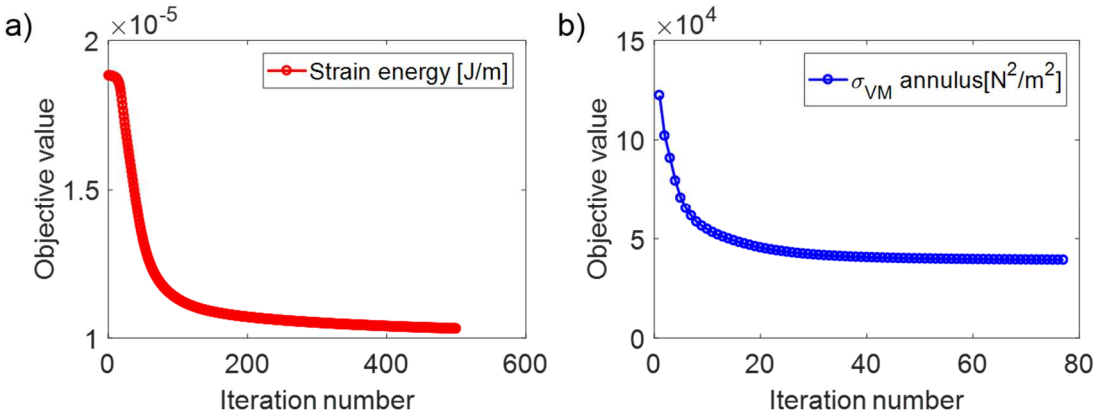


**Figure A5: Objective value as a function of iteration number** of 3D model for a) Strain energy and b) Von Mises stress.

**Stiffness/Elasticity matrix [MPa]**

$$C_{TI} = \begin{bmatrix} 2.4e5 & 1.1e5 & 1.4e5 & 0 & 0 & 0 \\ 1.1e5 & 2.4e5 & 1.4e5 & 0 & 0 & 0 \\ 1.4e5 & 1.4e5 & 2.0e5 & 0 & 0 & 0 \\ 0 & 0 & 0 & 1.3e5 & 0 & 0 \\ 0 & 0 & 0 & 0 & 1.3e5 & 0 \\ 0 & 0 & 0 & 0 & 0 & 6.4e4 \end{bmatrix}$$

$$C_{I} = \begin{bmatrix} 2.6e5 & 1.1e5 & 1.1e5 & 0 & 0 & 0 \\ 1.1e5 & 2.6e5 & 1.1e5 & 0 & 0 & 0 \\ 1.1e5 & 1.1e5 & 2.6e5 & 0 & 0 & 0 \\ 0 & 0 & 0 & 1.5e5 & 0 & 0 \\ 0 & 0 & 0 & 0 & 1.5e5 & 0 \\ 0 & 0 & 0 & 0 & 0 & 1.5e5 \end{bmatrix}$$